

An Extended Analysis of the BISRU Sled Tester's Dynamic Response

Kwame Boachie-Yiadom

September 2011

Supervisors:

Professor Gerald N. Nurick

Mr. Keith J. Balchin

**Dissertation submitted in partial fulfilment for the degree of
Master of Science in Mechanical Engineering**

Department of Mechanical Engineering at the University of Cape Town

Abstract

The BISRU (Blast Impact and Survivability Research Unit) Sled Tester is a deceleration sled testing system which will be utilised to test a range of mechanical components, including human surrogates under high decelerations, to understand the dynamic responses experienced. The commissioning phase of the Sled Tester project had begun at the beginning of this study and was nearing completion.

The limited space available to construct the Sled Tester system means that there are high accelerations experienced with a relatively low mass sled. The effects of inertial forces, caused by both the acceleration and deceleration phases on the components of the Sled Tester system, are of interest.

This study forms part of a larger project on the design of the Sled Tester system. A previous MSc. student, Patrick Smith, completed a study on the Sled Tester in 2009. At the beginning of the study, the rails, acceleration system (FESTO pneumatic cylinder) and deceleration system (MOOG hydraulic cylinder) had been completed. The Sled Tester utilises a control system with a PID controller. The contributions of Patrick Smith include the design of a seat in 2008 and a predictive numerical simulation which combined the pre-existing MOOG deceleration model and the FESTO acceleration model. This model included modifications to the pre-existing models provided and was able to predict the acceleration, velocity and displacement profiles for the acceleration and deceleration phases as well as the loading experienced by the sled. A conceptual design of the sled was proposed after a FEM model of the sled, payload and rail system was simulated using the loading profiles obtained from the combined and modified acceleration and deceleration numerical model.

The finite element method models run included a point mass for the surrogate and restraint system mass. The sled has a mass that is just over twice the mass of a surrogate. The masses of sled testers are typically in the region of 1ton, which is over twelve times the mass of a typical surrogate. The dynamics of the components and surrogate mounted on the sled will greatly influence the loading on the sled.

A model including a full surrogate model and fixtures to the sled, which would simulate a more realistic and common sled test scenario is proposed and completed in this study.

The finite element method model includes the sled as well as the seat which is elevated by a truss assembly to have the surrogate in a more realistic seated position. The seat and surrogate are allowed to slide forward with a slide mechanism that is designed to allow contact to occur on an impacting structure mounted on the sled during the deceleration event.

In order to perform a simulation of a crash test scenario, the surrogate had to be modelled and verified using pre-existing drop test data. The results of this model were satisfactory and a surrogate that had a response similar to reality was completed.

The simulations outputted results of the velocity and displacement profiles of the seat and surrogate during the deceleration and sliding phase. The results also included stress outputs, where the components were assessed under an elastic assumption only. The parts that were designed were adjusted in the light of the results of the simulations. The results showed no areas on the sled where the stresses reached a critical value for the material chosen and the testing scenarios simulated.

Plagiarism Declaration

"I know the meaning of plagiarism and declare that all the work in the document, save for that which is properly acknowledged, is my own"

K.A. Boachie-Yiadom

Signature.....

Date

Acknowledgements

The author would like to extend his appreciation and gratitude to the following people.

Prof. G.N. Nurick:

For his guidance and support throughout my stay at BISRU. His extensive experience in supervising and his knowledge of the field of structural impact were of great help during the course of my dissertation. I would like to extend my sincerest appreciation for all that he did for me during my stay.

Mr. K.J. Balchin:

For his technical experience and guidance, especially where the BISRU Sled Tester is concerned. I would like to say a special thank you for the optimism and encouragement that he showed me.

Mr. V.H. Balden:

For his input into FEM and specifically ABAQUS. Many hours were spent in consultation with him in discussing all my models and the development of them.

Mr. R. Govender:

For his technical input and guidance. Words cannot express the amount of help received and hours spent in constant discussion of every aspect of my project. My sincerest gratitude to him for all he did for me during my stay at BISRU.

Mr. P. Le Roux:

For his experience and guidance as far as the LMT surrogate leg was concerned.

CSIR (R. Ahmed and T. Pandelani):

For their help with the acquisition of data on the LMT surrogate leg and technical information received.

To my sister:

For her help in proof reading my dissertation and her endless supply of jollof rice.

To my brother:

For his support and encouragement throughout the duration of my Master's degree programme. I would like to say a special thank you to him not only for his guidance but also for setting such a high standard and great example for his younger siblings to follow.

To my parents:

For their constant commitment to excellence and their investment into my education throughout my life. I would also like to say thank you for their unwavering support and constant encouragement without the burden of pressure.

Table of Contents

Plagiarism Declaration	3
Acknowledgements.....	4
Table of Contents	6
List of Figures	12
List of Tables.....	22
Glossary of terms	24
1 Introduction.....	1
2 Background to the BISRU Sled Tester and its development.....	4
2.1 Rail system.....	4
2.2 Acceleration system	5
2.3 Deceleration system	6
2.4 Control system.....	7
2.5 Examples of similar sled testers and test setups.....	11
2.5.1 MESSRING compact sled testing systems.....	11
2.5.1.1 <i>Alternative MESSRING deceleration systems</i>	12
2.5.1.2 <i>Deceleration considerations of BISRU</i>	13
2.5.1.3 <i>MESSRING sled and mounted assemblies</i>	14
2.5.2 Wichita State University National Institute for Aviation Research (NIAR).....	14
2.6 The Politecnico di Milano Laboratory for the Safety of Transports.....	16
2.7 TRL Limited sled-based test rig.....	19
3 Previous work on the Sled Tester	22
3.1 Sled Tester seat design	22
3.2 Modelling of the system dynamics.....	25

3.3	Sled Design	29
3.4	Finite Element Method models.....	29
4	Literature on human surrogates.....	34
4.1	Overview of the anatomy of the leg and foot.....	34
4.2	Bones of the ankle and lower foot joints	35
4.3	Factors affecting the fracture of a bone in the lower leg.....	36
4.3.1	The Bone Mineral Density (BMD).....	36
4.3.2	Gender and Posture.....	36
4.3.3	Foot dynamics.....	37
4.4	Injury criteria for the lower limb	38
4.5	Anthropomorphic Test Devices	40
4.6	LMT surrogate leg.....	43
5	Discussion of design concepts.....	48
5.1	Wheel slide concept	51
5.2	Ertacetal C slide concept	52
6	Final designs	53
6.1	Base Elevation Structure (BES)	53
6.2	Bottom Slide Rail	56
6.3	Top Slide Flange.....	58
6.4	Foot Impactor (FI).....	61
7	Control study	62
8	Method of defining the FEM model	68
8.1	Introduction.....	68
8.2	Discussion of models created.....	68
8.3	Key ABAQUS theoretical concepts	70

8.3.1	Shell normals and shell offsets	70
8.3.2	Mesh size and stable time increment	71
8.3.3	Contact and interactions	73
8.3.3.1	<i>Surface to surface contact</i>	74
8.3.3.2	<i>General contact algorithm</i>	74
8.3.3.3	<i>Hard contact property (Normal force)</i>	74
8.3.3.4	<i>Penalty contact property (Tangential force)</i>	75
8.3.3.5	<i>Kinetic contact vs. penalty contact algorithm</i>	77
8.3.3.6	Slave and master surfaces	78
8.3.4	Mesh mapping algorithms.....	79
8.3.4.1	<i>Structured Meshing algorithm</i>	79
8.3.4.2	<i>Swept meshing (medial axis mesh algorithm)</i>	79
8.3.4.3	<i>Swept meshing (advance front mesh algorithm)</i>	79
8.3.4.4	<i>Free meshing (mapped on the boundaries)</i>	79
8.4	LMT Surrogate Leg model description	80
8.4.1	Geometry of model and its development	82
8.4.1.1	<i>Motivation for abandoning the beam element model</i>	86
8.4.1.2	<i>Solid LMT surrogate leg model</i>	88
8.4.1.3	<i>Rubber model</i>	89
8.4.2	Material properties and section assignments	95
8.4.3	Mesh	99
8.4.3.1	<i>Mesh types and sizes</i>	99
8.4.4	Assembly.....	106
8.4.5	Constraints.....	108
8.4.6	Interactions.....	108

8.4.6.1 Hip interactions	108
8.4.6.2 Knee Interactions	109
8.4.6.3 Ankle ball joint Interaction	110
8.4.6.4 Impacting surface interaction for the Drop Test	111
8.4.7 Loading	111
8.4.8 Predefined fields.....	112
8.4.9 Boundary conditions.....	113
8.5 Constrained sliding model with continuum element sled description (CSS)	114
8.5.1 Model Geometry	115
8.5.2 Material properties and section assignments	118
8.5.3 Mesh type and size	120
8.5.4 Assembly.....	122
8.5.5 Constraints.....	123
8.5.6 Interactions.....	124
8.5.7 Predicted fields	125
8.5.8 Boundary conditions.....	126
8.5.9 Loading	130
8.6 Description of BES Slide model with the Rigid sled (BSR)	130
8.6.1 Model Geometries.....	131
8.6.2 Materials and section assignments	134
8.6.3 Mesh	134
8.6.4 Assembly.....	138
8.6.5 Constraints.....	139
8.6.6 Interactions.....	140
8.6.7 Predicted fields	142

8.6.8	Boundary conditions.....	142
8.6.9	Loads.....	142
8.7	BES ABAQUS/Standard model description.....	143
8.7.1	Model geometry	144
8.7.2	Material properties and section assignments	144
8.7.3	Mesh	145
8.7.4	Assembly.....	147
8.7.5	Constraints.....	148
8.7.6	Interactions.....	148
8.7.7	Boundary conditions.....	150
8.7.8	Loads.....	150
9	Results and Discussion	152
9.1	LMT surrogate leg.....	152
9.1.1	Results of the beam element model	152
9.1.2	LMT surrogate leg force measurements.....	156
9.1.3	LMT surrogate leg foot development	159
9.1.4	Field output of the LMT surrogate leg drop test model	161
9.1.5	History output of the LMT surrogate leg drop test model	164
9.2	Constrained Slide with impactor on the Solid sled (CSS)	164
9.2.1	Dynamic and stress analysis	165
9.2.1.1	<i>3m/s Initial velocity test at 10g deceleration</i>	<i>165</i>
9.2.1.2	<i>4.7m/s Initial velocity test at 10g deceleration</i>	<i>170</i>
9.2.1.3	<i>5.7m/s Initial velocity test at 10g deceleration</i>	<i>174</i>
9.2.2	Stress analysis.....	178
9.2.3	Comparative results.....	180

9.3 BES Slide model with a Rigid sled (BSR)	183
9.3.1 5.7m/s Initial velocity test at 10g deceleration	183
9.3.2 History outputs of the 5.7m/s BSR model	187
9.3.3 Stress analysis	189
9.3.4 Deflection analysis	194
9.4 BES ABAQUS/Standard model	195
9.4.1 Stress analysis	195
9.4.2 Deflection analysis	198
10 Conclusions and Recommendations	199
11 References	203

List of Figures

Figure 2-1: Top view schematic of the BISRU Sled Tester	4
Figure 2-2: Rail system of the sled tester.....	4
Figure 2-3: The pneumatic acceleration system	5
Figure 2-4: The rear acceleration valves (left) and the frontal cushioning valves (right)	6
Figure 2-5: Hydraulic brake system of the sled tester	7
Figure 2-7: Schematic of the control operation of the deceleration of the sled [7].....	8
Figure 2-6: Example of an emergency stop	8
Figure 2-8: Picture of a MESSRING sled tester system taken from the deceleration end [9] ..	11
Figure 2-9: Schematic of MESSRING servo hydraulic crash testing system	12
Figure 2-10: Polyurethane (PU) tube braking	13
Figure 2-11: Schematic of steel bar braking	13
Figure 2-12: MESSRING crash test setup [9]	14
Figure 2-13: Wichita State University crash dynamics lab[11]	15
Figure 2-14: Wichita State University Crash Dynamic Laboratory, 60 Degree Pitch fixture [11].....	15
Figure 2-15: System trolley (left), oleo pneumatic brake system (right) [12]	16
Figure 2-16: Modified steel beam brake system.....	17
Figure 2-17: Results of the simulated, calculated and tested acceleration pulses - Target deceleration pulse (dash line), Mathematical model (black lines), FE simulation (dark grey line) and Actual test (light grey line).....	18
Figure 2-18: Idealised deceleration pulse of the footwell during a typical frontal impact [13]	19
Figure 2-19: Schematic of the TRL Limited sled test rig and mechanisms [13]	20
Figure 2-20: Mounting of the THOR-Lx in the same position as the cadaver leg tests [13] ..	21

Figure 2-21: Two repeat Hybrid III leg tests (left); two repeat cadaver tests using the sled test rig (right).....	21
Figure 3-1: Cone ASM on the left and Spline ASM on the right[2].....	22
Figure 3-2: Dog Clutch ASM [2].....	23
Figure 3-3: Seat in its two extreme positions [2].....	23
Figure 3-4: Base and backrest supports of the seat [2].....	24
Figure 3-5: Seat harness anchor points.....	25
Figure 3-6: Summary of the final sled velocity for the combination of the number of valves open and supply pressure[3].....	27
Figure 3-7: Final concept of the sled.....	29
Figure 3-8: Complete sled test model [3].....	30
Figure 3-9: Sled with point mass coupled to the surface [3].....	30
Figure 3-10: Figure illustrating the weak region (deceleration end) in the rail supports [3]	32
Figure 3-11: Rail system modified washer and stiffener.....	33
Figure 4-1: Ankle joint movement and foot anatomy [15].....	34
Figure 4-2: Bone structure of the lower leg and foot [15].....	35
Figure 4-3: Posterior(a), Distal (b) and Anterior (c) foot locations[19].....	37
Figure 4-4: Klopp et al. experimental setup [21].....	38
Figure 4-5: Bergeman and Prasad test setup [22].....	39
Figure 4-6: Hirsch criteria: Tolerance of stiff legged standing men to shock motion of short duration [24].....	40
Figure 4-7: Hybrid III dummy and THOR dummy [4],[26].....	42
Figure 4-8: LMT surrogate leg.....	43
Figure 4-9: LMT surrogate leg foot (Hybrid III 45° foot).....	43
Figure 4-10: LMT surrogate leg, lower ankle connection [14].....	44
Figure 4-11: Whyte test setups[16].....	45

Figure 4-12: Model of the lower leg of the LMT at 0 and 8ms [16]	45
Figure 4-13: Average peak loads for the LMT surrogate leg on the LLI at 3.4m/s (a) and 5.7m/s (b), plotted against PMHS data [27]	46
Figure 5-1: Test configurations in seated position on the left and flat position to the right.	48
Figure 5-2: Modified piston attachment for horizontal, flat test configuration	49
Figure 5-4: Seated test configuration with foot impact clamp	50
5-3: Seat configuration scenarios	50
Figure 5-5: Wheel slide, the assembly, the sliding platform and base slider respectively	51
Figure 5-6: Bottom Ertacetal slide concept (single piece)	52
Figure 6-1: Base elevation structure assembly	53
Figure 6-2: Critical areas of consideration in sizing the assembly	54
Figure 6-3: Seat and sled bolt connections.....	55
Figure 6-4: Bottom slide rail.....	56
Figure 6-5: Bottom slide assembly and bolt connections.....	56
Figure 6-6: Assembly of the slider prior to location (top) and after the top slider has been located (bottom).....	57
Figure 6-7: Bottom slide rubber fittings.....	57
Figure 6-8: Top slide flange	58
Figure 6-9: Completed designs prior to the start of this study.....	60
Figure 6-10: Complete assembly, seated position with additions.....	60
Figure 6-11: Impact lower leg clamp: first amendment (left); final design (right)	61
Figure 6-12: Impact plate assembly	61
Figure 7-1: Schematic of the deceleration cylinder	64
Figure 7-2: Effective pressure control logic [7]	64
Figure 7-3: Sled force schematic diagram.....	65

Figure 7-4: Steady state response graph[32]	67
Figure 8-1: Schematic of shell offsets	70
Figure 8-2: Graphical illustration of shell offsetting methods	71
Figure 8-3: Coulombs static friction graph [33]	75
Figure 8-4: ABAQUS static/dynamic exponential decay graph [34].....	76
Figure 8-5: Schematic of master/slave node and surface penetration.....	78
Figure 8-6: Composite body part	82
Figure 8-7: LMT surrogate leg model wire frame (a) and rendered beam elements (b).....	82
Figure 8-8: Foot revision one (a) and HUMANETICS Hybrid III 45°foot CAD drawing (b) [36]	83
Figure 8-9: LMT surrogate leg surface interaction at the knee hinge [37]	84
Figure 8-10: Hip hinge joint model (a) and LMT CAD drawing (b) [37]	85
Figure 8-11: Composite body final isometric view (a) LMT CAD isometric (b); side view (c) and CAD side view (d) [37]	86
Figure 8-12: Hinge geometric assignment schematic.....	87
Figure 8-13: Deceleration phase model of the beam element LMT surrogate leg.....	87
Figure 8-14: Femur FEM model (a); original CAD drawing (b) [37]	88
Figure 8-15: Tibia model revision 1 (a); CAD drawing (b); and section view AA (c)[37].....	89
Figure 8-16: Mooney-Rivlin constants vs. Shore Hardness graph	93
Figure 8-17: Modifications to the surrogate leg rubber foot and ankle connections(a), HUMANETICS CAD drawing (b) and tibia ball joint (c) [36]	94
Figure 8-18: Rigid impact surface for the drop test.....	94
Figure 8-19: Hip and knee pin.....	95
Figure 8-20: Washers; knee outer (a) and inner (b) and hip outer(c) and inner (d).....	95
Figure 8-21: Material assignment for the composite body	97
Figure 8-22: Material assignment for the outer washers	97

Figure 8-23: Material assignment for the hip and knee pins.....	98
Figure 8-24: Material assignment for the tibia	98
Figure 8-25: Composite Body mesh (a) and partition strategy (b)	100
Figure 8-26: Femur mesh.....	101
Figure 8-27: Tibia mesh partitions and mapping algorithms.....	102
Figure 8-28: Foot ankle connector mesh and partitioning strategy	103
Figure 8-29: Foot rubber mould partitions.....	103
Figure 8-30: Foot rubber mould mesh.....	104
Figure 8-31: Hip and knee pin mesh	104
Figure 8-32: Washer meshes	105
Figure 8-33: LMT surrogate leg model assembly.....	106
Figure 8-34: Original CAD assembly of hip joint (a) and knee joint (b)[37].....	107
Figure 8-35: FEM assembly of hip joint (a) and knee joint (b).....	107
Figure 8-36: Ankle joint FEM assembly.....	107
Figure 8-37: Graphical representation of hip hinge joint interactions; washer surfaces (a) and pins (b).....	109
Figure 8-38: Graphical representation of knee hinge joint interactions.....	110
Figure 8-39: Graphical representation of ankle ball joint interaction	110
Figure 8-40: Graphical representation of drop test impacting surface interaction	111
Figure 8-41: Bolt load definition on the knee (a) and hip joints (b).	112
Figure 8-42: Seat geometry.....	115
Figure 8-43: FI angle iron support (a) and inclined impactor (b).....	115
Figure 8-44: FI first revision	116
Figure 8-45: Plate deformation on the FI first revision.....	117
Figure 8-46: Final revision of the FI.....	117

Figure 8-47: Entire sled excluding the rail slides (a); sled included in the model after cut extrusion (b)	118
Figure 8-48: Seat section assignments	119
Figure 8-49: Sled bolt material assignment partition	120
Figure 8-50: Seat mesh	121
Figure 8-51: FI mesh (a) and partitioning and mapping strategy (b).....	121
Figure 8-52: Solid frontal sled mesh	122
Figure 8-53: Assembly of the free sliding model	122
Figure 8-54: LLI testing of the LMT surrogate leg (a) and Hybrid III (b) [16].....	124
Figure 8-55: FI interaction (orange) and sled interaction (green)	124
Figure 8-56: Solid sled boundary axial condition.....	126
Figure 8-57: 17m/s velocity and deceleration profile.....	127
Figure 8-58: Idealised frontal impact footwell deceleration pulse (a) and actual pulse from tests conducted (b)[13]	128
Figure 8-59: Velocity profile of a 10g constant deceleration pulse	130
Figure 8-60: Rigid sled planar shell with bolt extrusions.....	131
Figure 8-61: Square tube profile (a) and extrusion lengths (b)	132
Figure 8-62: Angle Iron flange profile (a) and part extrusion (b).....	133
Figure 8-63: Bottom slide bottom half (a) and angle irons (b)	133
Figure 8-64: Outer truss (a) and inner truss (b).....	134
Figure 8-65: Rigid sled mesh	135
Figure 8-66: BES mesh (a) and partition and mapping strategy (b).....	135
Figure 8-67: Bottom slide angle iron.....	136
Figure 8-68: Top slide mesh	136
Figure 8-69: Back rubber stopper mesh	137

Figure 8-70: Front rubber stopper mesh	137
Figure 8-71: Inner and Outer truss mesh.....	138
Figure 8-72: BES slide rigid sled model assembly	138
Figure 8-73: BES sled model assembly clearance	139
Figure 8-74: BES slider model constraints; FI bolts (a), BES bolts (b) and top slide bolts (c)	140
Figure 8-75: Bottom slide bolts interactions.....	141
Figure 8-76: Slider interactions.....	141
Figure 8-77: BES slide model rubber interactions.....	142
Figure 8-78: Sled shell rigid surface	144
Figure 8-79: BES ABAQUS/Standard mesh (a) and mesh based on partitions (b).....	146
Figure 8-80: ABAQUS/Standard bottom slide angle iron mesh	146
Figure 8-81: ABAQUS/Standard rigid sled mesh.....	147
Figure 8-82: BES assembly – isometric view (a) and side view (b)	147
Figure 8-83: BES bolt surface tie constraints	148
Figure 8-84: Bottom slide bolt interactions	149
Figure 8-85: BES and sled interaction	149
Figure 8-86: BES standard model load assignments.....	150
Figure 9-1: Constrained slide model with beam element LMT surrogate leg, with rubber stoppers	153
Figure 9-2: Velocity history of constrained slide beam element model for a friction coefficient of 0.3.....	154
Figure 9-3: Velocity history of constrained slide beam element model for a friction coefficient of 0.9.....	155
Figure 9-4: Strain gauge location on the LMT surrogate leg (a) and schematic detailing the locations of all gauges (b)	156

Figure 9-5: Element locations where strain readings were outputted on the tibia load cell section	157
Figure 9-6: Strain gauge schematic of the circuit (a) and single bridge configuration (b)...	158
Figure 9-7: Foot steel plate with pin ankle joint	159
Figure 9-8: Foot plate with rubber pad and pin ankle joint.....	160
Figure 9-9: 8 discrete field output plots of the LMT surrogate leg model drop test.....	162
Figure 9-10: Field output showing the Von Mises stress in the LMT surrogate leg model .	163
Figure 9-11: Tibia load for a drop test with an impact velocity of 3.13 m/s.....	164
Figure 9-12: Field output for the CSS 3m/s test.....	167
Figure 9-13: Velocity histories (a) and displacement histories (b) for the seat and sled for the 3m/s test	168
Figure 9-14: Relative displacement of the seat and sled for the 3m/s CSS model.....	169
Figure 9-15: Kinetic and Frictional energy dissipation plot of the 3m/s CSS model.....	169
Figure 9-16: Field outputs for the 4.7m/s CSS model.....	171
Figure 9-17: Velocity histories (a) and displacement histories (b) for the seat and sled for the 4.7m/s test	172
Figure 9-18: Relative displacement between the seat and sled for the 4.7m/s CSS model	172
Figure 9-19: Kinetic and Frictional energy dissipation plot of the 4.7m/s CSS model.....	173
Figure 9-20: Field output for the 5.7m/s CSS model	175
Figure 9-21: Velocity histories (a) and displacement histories (b) for the seat and sled for the 4.7m/s test	176
Figure 9-22: Relative displacement between the seat and sled for the 5.7m/s CSS model	177
Figure 9-23: Kinetic and Frictional energy dissipation plot of the 5.7m/s CSS model.....	177
Figure 9-24: FI maximum stress field output (isometric rear view)	179
Figure 9-25: FI maximum stress field output (isometric front view)	179
Figure 9-26: Sled maximum stress field output	179

Figure 9-27: Comparative plots of the seat velocity for the three test scenarios	180
Figure 9-28: Comparative plots of the seat displacement for the three test scenarios	181
Figure 9-29: Comparative plots of the seat velocity vs. maximum relative displacement of the sled for the test scenarios	181
Figure 9-30: Final zero velocity positions of the seat and surrogate for the three test scenarios.....	182
Figure 9-31: Plot of the frictional energy dissipation for the three test scenarios.....	182
Figure 9-32: Discrete field outputs illustrating the simulation dynamics.....	187
Figure 9-33: Velocity (a) and displacement histories (b) for the seat and sled for the 5.7m/s BSR test.....	187
Figure 9-34: Relative displacement plot of the 5.7ms test for the BSR model.....	188
Figure 9-35: Von Mises field output stress of the BES (side view)	190
Figure 9-36: Von Mises field output stress of the BES (isometric view)	190
Figure 9-37: Bottom square tube contact with top sled surface	191
Figure 9-38: Zoomed-in figure of the Von Mises field output stress of the BES	192
Figure 9-39: Bottom slide angle iron: Von Mises field output stress.....	193
Figure 9-40: Top slide angle iron: Von Mises field output stress	193
Figure 9-41: Bottom slide angle iron: peak deflections from the front sliding shoes	195
Figure 9-42: Von Mises field output stress for the BES standard model: (a) side view and (b) isometric view.....	197
Figure 9-43: Von Mises field output stress for the bottom slide angle iron, standard model	197
Figure 9-44: Deflection field output in they-direction of the bottom slide angle iron, standard model.....	198
Figure 10-1: Standard seating position in automobiles.....	200
Figure A-1: Ertacetal C Copolymer datasheet [29]	208

Figure A-2: Steel bolt mechanical datasheet [44].....	209
Figure A-3: VRN T690 steel datasheet [51].....	210
Figure A-4: EN19 Condition V datasheet [31].....	210
Figure A-5: Stainless steel datasheet (U-2001) [30]	211
Figure A-6: Strain gauge bridge configuration diagrams and calculations (page1) [49].....	214
Figure A-7: Strain gauge bridge configuration diagrams and calculations (page2) [49].....	215
Figure A-8: BES angle iron mounting flange moment schematic	217
Figure A-9: Schematic of moments experinced by the BES during the acceleration phase	219
Figure A-10: Bottom slide loads during acceleration.....	221
Figure A-11: bottom slide bolt loading	222
Figure A-12: Top slide shoe bolt load diagram.....	224
Figure A-13: Top slide shear loading	225
Figure A-14: Top slide bolt holes experiencing shear during the sliding motion	225
Figure A-15: Schematic of top slide cg distances.....	226
Figure A-16: Bottom slide schematic of the load on the rubber cushion.....	227

List of Tables

Table 2-1: Optimised deceleration control parameters [3]	10
Table 3-1: CADM acceleration outputs	27
Table 3-2: CADM acceleration variables plotted.....	27
Table 3-3: CADM deceleration outputs.....	28
Table 3-4: CADM deceleration variable plots	28
Table 4-1: Axial force limits in the tibia arranged by age[16]	36
Table 4-2: Mechanical strength of bone in the lower leg[16].....	36
Table 4-3: List of commonly used ATDs[25]	41
Table 4-4: Response of the LMT surrogate leg on the LLI for varied spring preload stiffnesses and peak plate velocities[28].....	47
Table 7-1: Optimised input parameters[7].....	62
Table 8-1: Mooney-Rivlin deviatoric strain constants.....	92
Table 8-2: Moduli conversion table [42]	93
Table 8-3: LMT surrogate leg model material properties	99
Table 8-4: Loading parameters for LMT surrogate leg bolt clamp loads	112
Table 8-5 Materials properties used in the LMT surrogate leg model.....	119
Table 8-6: Deceleration profile of an initial velocity of 5.7m/s and 10g deceleration	129
Table 8-7: BES material properties.....	144
Table 8-8: BES standard model load assignment magnitudes	151
Table 9-1: Beam element slide impact model parameters and test conditions for test 1 ..	154
Table 9-2: Beam element slide impact model parameters and test conditions for test 2 ..	155
Table 9-3: 3m/s CSS results	166
Table 9-4: 4.7m/s table of results	170

Table 9-5: 5.7m/s CSS model table of results	174
Table 9-6: Maximum Von Mises stress for the FI and sled	178
Table 9-7: Table or results for the 5.7m/s BSR model.....	185
Table 9-8: Maximum stress results obtained with the BSR model	194
Table 9-9: BES standard model stress results	196
Table A-1: Coefficient for static friction of steel [44]	212
Table A-2: Static and sliding friction table [45]	213
Table A-3: Mass and accelerations values for the designed parts.....	218
Table A-4: Cg distances from the BES angle iron mounting flanges	219
Table A-5: BES angle iron flange bolt information	220
Table A-6: Bottom slide cg and moment distances.....	221
Table A-7: Bottom slide angle iron cross sections and loading experienced	222
Table A-8: Fillet weld dimensions on the bottom slide	223
Table A-9: Top slide shoe load and bolt values	224
Table A-10: Top slide flange vertical support load and cross section information	224
Table A-11: Top slide bolt information.....	226
Table A-12: Rubber stopper dimensions and load.....	227

Glossary of terms

ASM:

Angle Selection Mechanism – A mechanism used for the angle adjustments of the Sled Tester seat.

ATD:

Anthropomorphic Testing Device – A surrogate testing device that aims to replicate the dimensions, weight and movement of a human being.

BES:

Base Elevation Structure – A box shaped truss structure used to elevate the Sled Tester seat which is mounted on the sled. This is in order to have a surrogate in a seated position.

BISRU:

Blast Impact and Survivability Research Unit – The Sled Tester is housed at BISRU.

BSR:

BES and Slider with impactor on the Rigid sled model – A model that includes the BES and Slider with an unconstrained rigid seat. The sled is modelled as a rigid body with shell elements onto which the foot impactor is mounted.

CADM:

Combined Acceleration and Deceleration stage Model – A numerical model created in MATLAB that models the Sled Tester system for the entire sequence of operation. Acceleration and deceleration outputs are obtained from this model for given input parameters.

CSIR:

Council for Scientific and Industrial Research – A facility where tests were previously conducted on the LMT surrogate leg.

CSS model:

Constrained Slide with the impactor on the Solid sled model – A model that includes the rigid seat constrained to move only in the direction of motion of the sled. The sled is modelled as a 3D continuum element body, onto which the foot impactor is mounted.

E-Stop:

Emergency stop – An electrical switch used to cut off the electrical power immediately when activated.

FEM:

Finite Element Method – A mathematical system and technique that finds approximate solutions for partial differential equations and integral equations.

FI:

Foot Impactor – An impacting surface mounted on the sled to replicate a footwell. Impact will result at the foot/feet of a surrogate during a deceleration test.

LMT surrogate leg:

Land Mobility Technologies surrogate leg – A surrogate leg designed by Land Mobility Technologies (Pty) Limited, which includes a femur, tibia and foot representation.

PID Controller:

Proportional, Integral and Derivative controller – A control loop feedback system that calculates its error by summing up the proportional, integral and derivative value of the error associated with the system.

PLC:

Programmable Logic Controller – A programmable digit computer capable of monitoring and controlling industrial processes and systems.

PMHS:

Post Mortem Human Subject – Human cadavers or limbs subjected to testing for research purposes.

SCADA:

Supervisory Control and Data Acquisition – A computer system that forms the interface between the control systems and operating equipment. The system is responsible for storing all the data required for the industrial system in use.

Seeding

The manner in which the nodes of the elements of a body are placed and arranged. The elements can be arranged in a manner in which the nodes are evenly spaced away from one another or can be altered to be spaced according to the user's specifications.

Von Mises Stress

A failure theory used to determine the applied stress in a member. It combines principal stresses, from Mohr's Circle (bending & torsion), into an equivalent applied stress which is compared to the allowable stress of the material.

1 Introduction

At the Blast Impact and Survivability Research Unit (BISRU), the primary areas of interest are the effects of blast and impact loading on persons, structures and vehicles. The BISRU Sled Tester at the University of Cape Town is an experimental rig that can simulate a high deceleration event. The tests and experiments to be performed on that rig will aid in mitigating injuries and damage to persons and equipment, by understanding the dynamic responses experienced on the test specimens during a high deceleration event. The Sled Tester will be used to test a range of specimens and mechanical components, including human surrogates. The BISRU Sled Tester will add additional value to the field of structural impact. Up until now, the methods of impact testing were performed on drop testers and an apparatus called a Split Hopkinson Pressure Bar. These all have their limitations. One of the limitations is the g-force levels that are achievable (1g) and another is the size of the specimens that can be tested.

The Sled Tester project has been an ongoing project with previous students having contributed to it. The primary reason why this Sled Tester system was designed was to investigate the effect of high decelerations on anthropometric test devices (ATDs). These include fully instrumented crash test dummies such as the Hybrid III and THOR dummies, as well as other surrogate devices such as the Land Mobility Technologies (LMT) surrogate leg. At the beginning of the study, BISRU did not own a Hybrid III crash test dummy. The LMT surrogate leg was used instead to assess all the designed parts for the Sled Tester by means of computational simulations. The possibility of assessing the validity of using ATDs under blast loading exists with the current setup of the BISRU laboratory. The results from blast tests can be correlated with the horizontal loading of an ATD on the Sled Tester. ATDs are more often than not used and tuned for seated frontal, rear or side loading configurations.

The Sled Tester project is approaching the final stages of commissioning, where certain aspects need to be assessed. These include the design of all components necessary to perform a full deceleration test that replicates a real life situation. Models that predict the responses of the sled and rail system with these fixtures were simulated in ABAQUS version 6.10-1 (FEM package).

The Sled Tester consists of a sled, located and mounted on a rail system. The sled and its payload travel between two cylinders, one that accelerates the sled and its payload and the other that performs the deceleration. One of the major constraints of this system is the shortage of space available to construct the Sled Tester. The area allocated for the project was approximately 14m long by 5m wide. Typically, sled testers of this type have at least double the space in which to operate (for example, the 36m long by 7m wide MESSRING Compact Sled Testing Systems[1]). This poses an interesting set of challenges because the space is so limited and therefore the mass of the sled and payload will have to be limited and consequently, will be subjected to high g-forces. Another key limitation is cost: this constraint affected every component and design. The dynamics and strength of the design need to be critically assessed to expose any weakness at any stage of the design and to determine any possible issues that may arise.

A customised pneumatic cylinder was designed by FESTO to enable the sled to be accelerated to the desired velocities. The FESTO cylinder can accelerate the sled and payload (totalling 300kg) from rest to 17m/s with a maximum peak acceleration of just over 14g. The sled will disengage from the piston and will travel along the rails and make contact with the hydraulic cylinder designed by HYFLO. The deceleration system allows for decelerations up to 59g. However, the sled seat designed by Smith [2] can only withstand a maximum deceleration of 36g. This seat could not be designed to withstand higher g-forces, given the weight restrictions applicable to that assembly. Nonetheless, it is unlikely that testing that requires the use of the seat will reach g-force levels higher than 36g. The deceleration event in particular had to be controlled with a highly sophisticated control system which was contracted out to HYFLO.

It is at this stage relevant to discuss where this project's position lies relative to previous work and possible future work. At the beginning of this study, the designs and mounting of the pneumatic and hydraulic actuators had been completed. The rail system had been completed with a few minor components still to be added. The modelling of the deceleration stage had been completed by the suppliers. Work on the control system is ongoing with most of it being completed already.

The work completed by Smith [2] in 2008 entailed the design of a seat to be mounted onto the sled. In 2009 a computational model based on the pre-existing FESTO model of the

pneumatic acceleration stage was completed. This model was more comprehensive and detailed than the FESTO model which predicts the velocity profile of the sled during the acceleration stage only. This was combined with the pre-existing deceleration stage model created by MOOG. The outputs from this model were then used in assessing the structural response of the rail system and a workable conceptual sled design was analysed using a finite element model. Smith [3] created models of the sled and rail system, which included the effective mass of a 50th percentile Hybrid III male dummy. The mass was positioned at the combined centre of the mass of the dummy and restraint system. This was modelled as a point mass on the sled with a distributed couple. One of the key outcomes of this model was not only the optimisation of the sled design but Smith [3] also found areas of structural weakness at the deceleration end of the rail supports. In particular, the rail supports were not stiff enough for the loads and moments that would be experienced. Stiffer supports have been installed as a result of the recommendations proposed by him.

For the purpose of this dissertation, the following aspects will be investigated and accessed.

Building on from a previous student's work

As an extension to the dissertation completed by Smith [3], adjustments, additions or modifications to designs will be explored if and when the need arises. This will allow an overall assessment of the response of the Sled Tester system for a full scale test to be made.

Development of a FEM model of the system

Building on from Smith [3], where a FEM model of the interactions between the sled, rails and the supporting structures was created: the sled has a mass comparable to that of the ATD dummy ($\pm 170\text{kg}$ - sled vs. 77.7kg - ATD [4]). Typical sled masses are in the region of 1ton. The dynamics of the dummy will heavily influence the response of the sled and the Sled Tester system. As opposed to using a point mass, a FEM model is created in which a LMT surrogate leg is secured to a seat fixed onto the sled itself. The results are compared to those included in the literature, bearing in mind that the BISRU Sled Tester has some significant differences which may affect the results. The most notable of these differences is the direction of loading.

2 Background to the BISRU Sled Tester and its development

The schematic in figure 2-1 shows an overview of the Sled Tester and each of the different highlighted systems will be discussed and elaborated on, in this Chapter.

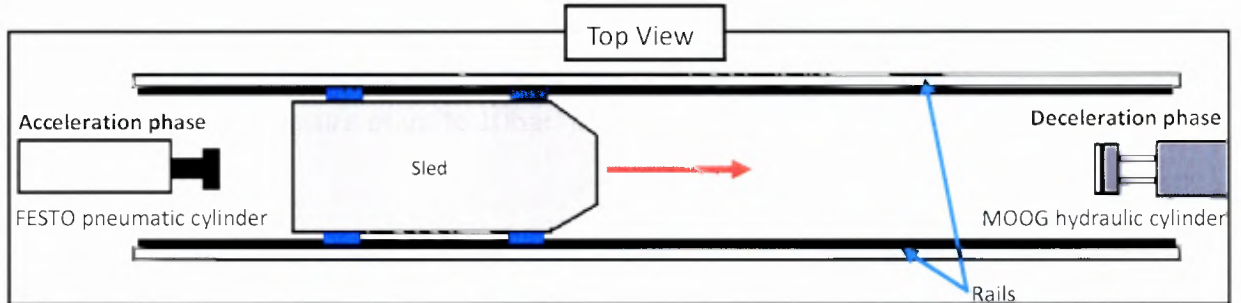


Figure 2-1: Top view schematic of the BISRU Sled Tester

2.1 Rail system

The rail system lies between the pneumatic acceleration cylinder and the hydraulic deceleration cylinder. The steel sliding rails run along the mild steel channel sections that are bolted to each other and bolted to the ground (see figure 2-2). The rails are reinforced at the deceleration end with stiffener supports to give greater rigidity to the structure and system.

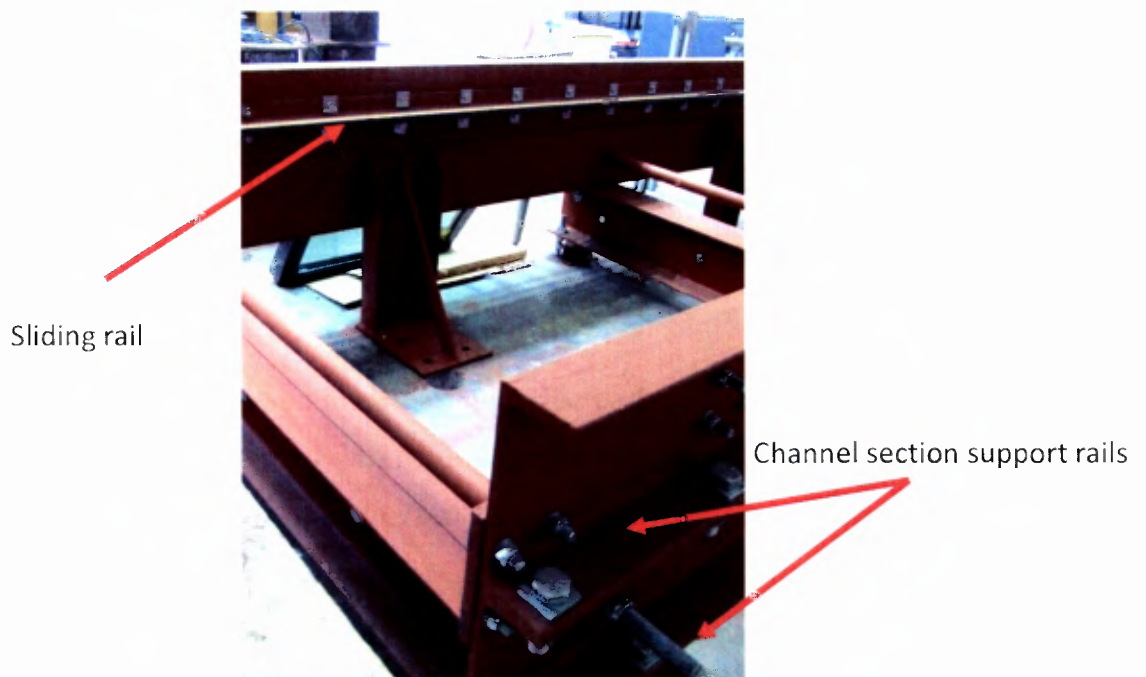


Figure 2-2: Rail system of the BISRU Sled Tester

2.2 Acceleration system

The sled is propelled by a customised pneumatic cylinder designed by FESTO. The cylinder is capable of accelerating the sled to a peak velocity of 17m/s [5]. The peak acceleration is 14g. The cylinder has a bore of 250mm and a working stroke of 2.5m. Air is compressed in a compressor after which it is filtered and sent to a large air receiver which supplies the cylinder with air at a pressure of up to 10bar. The acceleration system can be seen in figure 2-3.

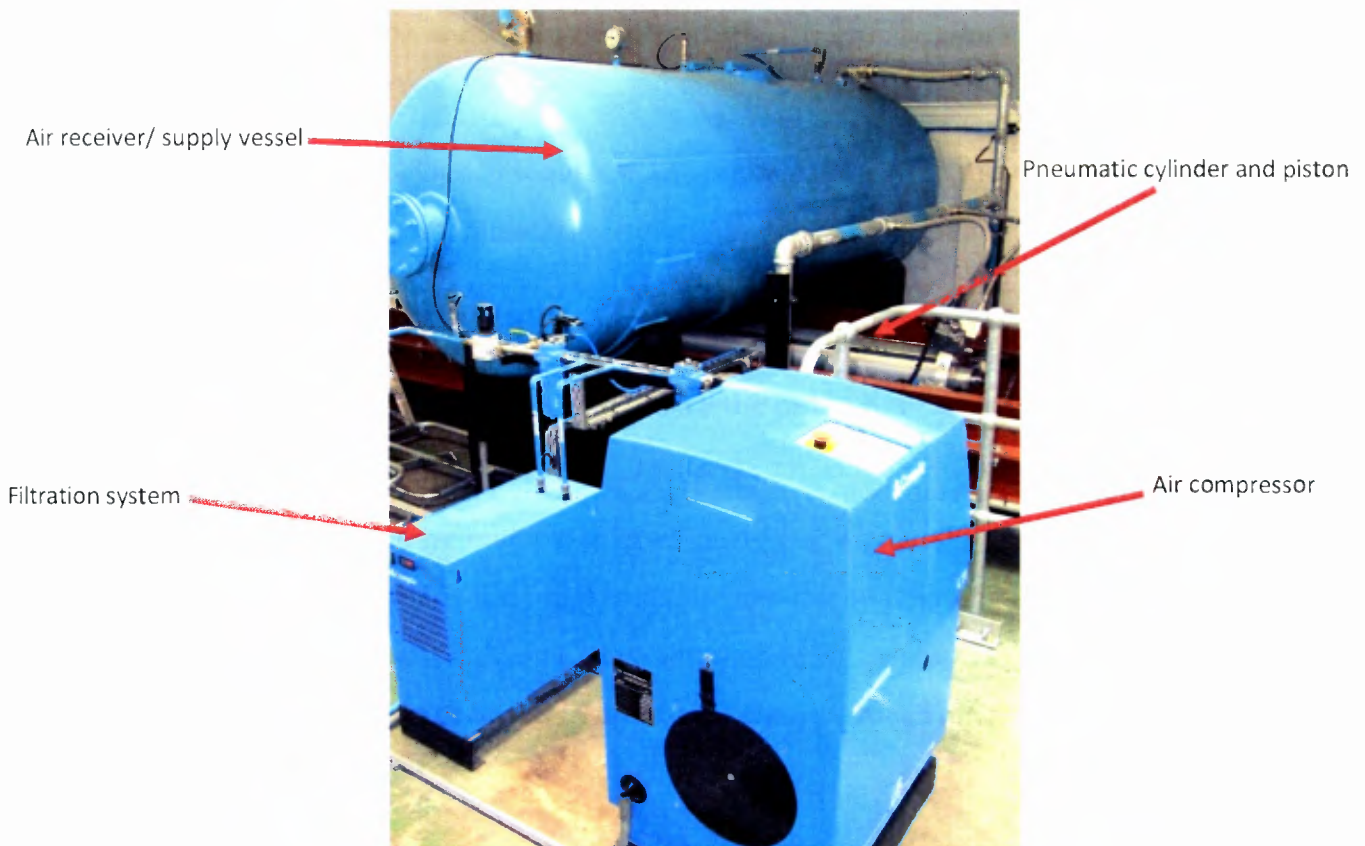


Figure 2-3: The pneumatic acceleration system

The original design brief allowed for a maximum sled and payload of 250kg and a desired peak velocity of at least 60km/h which corresponds to 16.7m/s [6]. The maximum sled mass and payload was later increased to 300kg. A very high flow rate is required for the piston to reach the desired accelerations. A single large inlet valve could not be made to achieve this and to overcome the problem, customised end caps were machined at both ends of the cylinder. There are twelve inlet ports and six outlet ports (see figure 2-4). Solenoid valves are mounted adjacent to these ports.

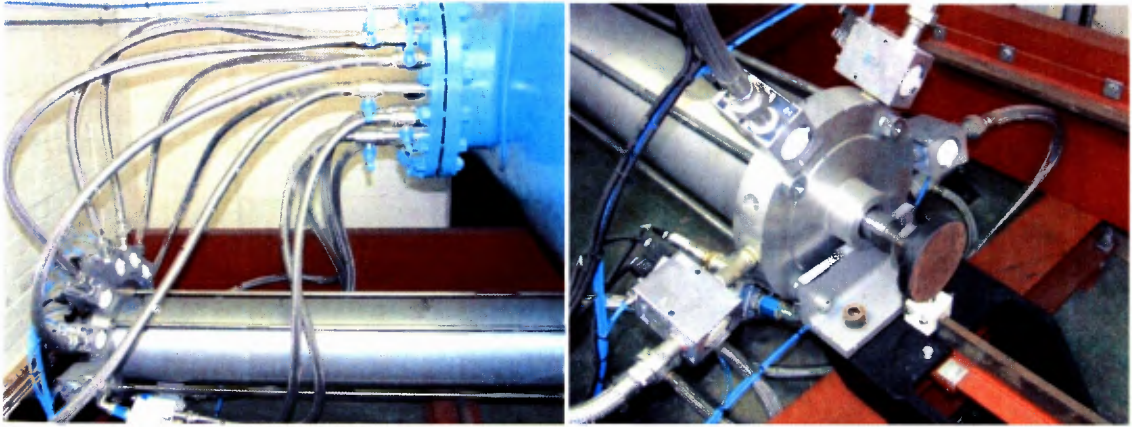


Figure 2-4: The rear acceleration valves (left) and the frontal cushioning valves (right)

Upon activation of the launch sequence, the pressurised air fills the rear chamber through the inlet valves. This compressed air displaces the piston. Once the desired sled velocity is reached, the supply air is switched to the outlet valves which pressurise the front chamber of the cylinder to decelerate the piston. Cushioning air also ensures that the piston does not impact the front end of the cylinder. Once the piston has begun to decelerate, the sled disengages from the piston head.

Another benefit of having multiple inlet valves is that a greater variation of accelerations can be achieved by varying the supply pressure and the number of valves open for the rear chamber. It must be noted that all six valves need to be activated during each test for the front chamber. This is to prevent any air from escaping through an inactive valve during the cushioning of the piston.

2.3 Deceleration system

The deceleration is controlled by means of a servo hydraulic system. The hydraulic piston is aligned so that contact with the front of the sled is made during the deceleration sequence. The entire design and construction of the deceleration system was done by HYFLO. A hydraulic cylinder was chosen because of the high pressures available to such systems and its ability to have varied decelerations.

The hydraulic cylinder has a bore of 100mm and a working stroke of 1.1m. The system is capable of achieving a 59g deceleration for a maximum payload of 300kg [7]. The deceleration system can be seen in figure 2-5.

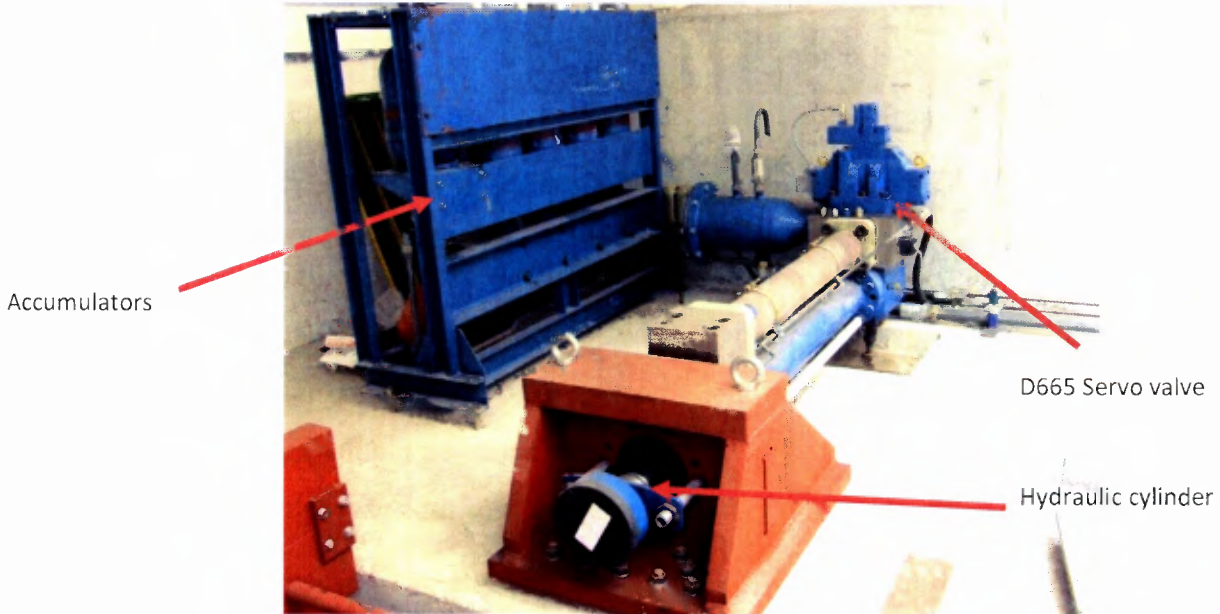


Figure 2-5: Hydraulic brake system of the BISRU Sled Tester

At the deceleration stage, the hydraulic cylinder's motion is controlled by a high speed servo valve (D665), a set of accumulators, a hydraulic power pack and a control unit connected to the Programmable Logic Controller (PLC).

2.4 Control system

The system utilises a PID controller to control the deceleration sequence. A central control unit (CCU) allows the acceleration and deceleration systems to communicate. This unit also manages the different interlock mechanisms to ensure the safe operation of the Sled Tester. The unit is operated via a SCADA system to which all inputs are sent. This SCADA system controls all the relevant parameters through the PLC, which performs all the necessary safety checks for the entire system before it allows the sequence to run. Various emergency stops (E-stops) are fixed at certain points to stop the operating sequence and to place the system in a safe mode when activated. An example of one such E-stop is shown in figure 2-6.

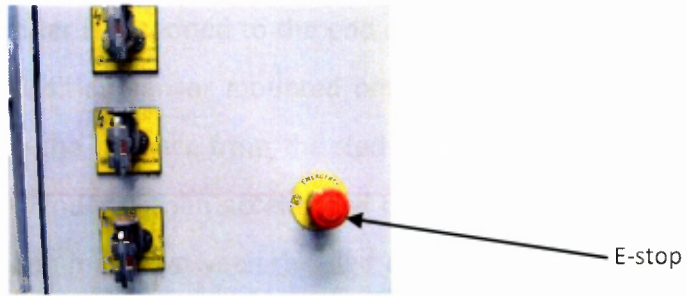


Figure 2-6: Example of an emergency stop

An uninterrupted power supply (UPS) is fitted to safeguard against any power cuts. The UPS also supplies the PLC which contains two DC power supplies that energise the solenoid valves and other components of the system. Redundancies are created with the supply of power by using multiple power supplies. Each power supply is capable of running the entire system and in this way adds to the safe operation of the system [3].

Figure 2-7 shows a schematic of the operation of the control system at the deceleration end of the Sled Tester system. There are two pressure sensors in the front (P_b) and rear chamber (P_a). There is a position sensor on the cylinder (X_c) and a position sensor on the sled (X_s).

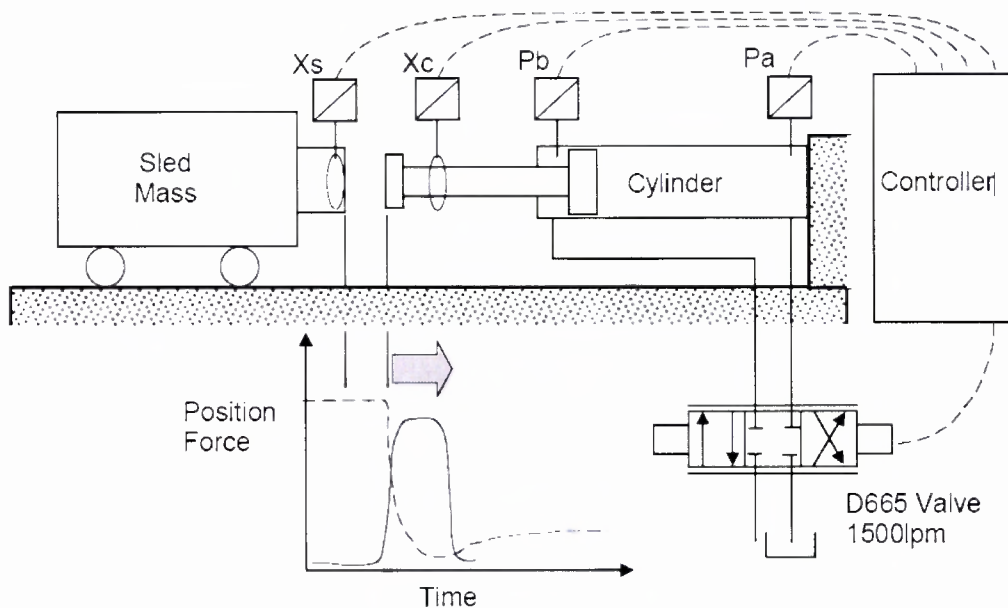


Figure 2-7: Schematic of the control operation of the deceleration of the sled [7]

Before the sled is fired, the cylinder is extended to the end of its stroke. The sled's velocity and position are tracked by a position sensor mounted onto the sled. A pre-acceleration distance is prescribed and when the distance from the sled and piston has reduced to the pre-acceleration distance, the cylinder is then accelerated to match the incoming velocity of the sled. Once contact has been made between the sled and the piston, the control unit switches from position control, to pressure control. The control unit regulates the cylinder to match the desired set point pressure and control parameters. The deceleration sequence exerts a force on the sled, from the backpressure of the hydraulic cylinder, and therefore slows it down.

The force on the cylinder is calculated indirectly from the measurements obtained from the pressure transducers on the rear and front of the cylinder. The values obtained by these pressure transducers are used to derive the effective pressure (equivalent to the force/bore area) of the cylinder. This information is then tracked back to the control unit and used to regulate the amount of hydraulic fluid in the cylinder. The controller attempts to maintain the desired force required to slow the sled down at a steady and constant rate.

The purpose of the two position sensors is to indicate the trigger point for when the cylinder will be retracted before contact. The acceleration of the cylinder will be determined by the incoming velocity of the sled. When the release logic (RL) holds false, the control unit will be operating under position control conditions and will switch to pressure control when the RL holds true.

The parameters to be set for the controller are the effective target pressure, the pre-acceleration distance and the sled mass. These values are then used in a spreadsheet to derive new parameters for the control release logic and ramp functions. These new and derived parameters are the valve opening (area), pre-acceleration distance and ramp closing time. At high loads apart from these parameters, the damping in the PID controller needs to be increased to ensure adequate control of the system. The pre-acceleration distance is proportional to the contact velocity and will reach a negative value if the kinetic energy does not create the minimum required pressure on the cylinder. A 3m/s contact velocity was seen to be a lower limit contact velocity given a sled mass of 250kg in a study performed by MOOG [7].

The system parameters for an ideal test are tabulated in table 2-1.

Table 2-1: Optimised deceleration control parameters [3]

System Specifications Optimized control parameters	
Supply Pressure (Ps)	350 bar
Bore Diameter	100 mm
Rod Diameter	75 mm
Stroke	1100 mm
Cylinder Operating Point	1000 mm
Rod Side Additional Volume	8 litres
Bore Side Additional Volume	2 litres
Fluid Modulus	0.7 GPa
Input Parameters	
Target Effective Pressure (Pt)	100 bar
Sled Contact Velocity (V)	17 m/s
Sled and Rod Mass (M)	340 kg
Control Parameters	
Stiffness (K)	5372.5 N/mm
No Flow Displacement (No)	14.6 mm
Valve Ramp Start Area (At)	9 V
Pic acceleration Distance (No)	89 mm
Valve Ramp Rate Closing Time (Tc)	0.105 ms

2.5 Examples of similar sled testers and test setups

In this section, some of the sled testers that exist around the world and that are utilised in a similar manner to the BISRU Sled Tester, are discussed. This discussion provides some insight into the difficulties associated with sled testing and also reviews the technologies available for sled testing.

2.5.1 MESSRING compact sled testing systems

MESSRING is a company based in Germany that has been in operation for over 40 years [8]. The company's areas of expertise lie in setting up and installing compact sled testing systems. They also provide data acquisitions systems as well as software and transducers. Currently they have over 90 crash testing facilities around the world [8]. An example of a MESSRING sled testing system is shown in figure 2-8.



Figure 2-8: Picture of a MESSRING sled tester system taken from the deceleration end [9]

The sled is accelerated by a servo hydraulic motor via a drive chain. The maximum payload for the system is 1000kg, allowing the sled to reach a maximum speed of 80km/h. The

space requirement for the installation of a MESSRING sled tester is ideally 36m long by 7m wide [1].

There are a number of braking techniques that the company can provide, the most typical of which is shown in figure 2-9.

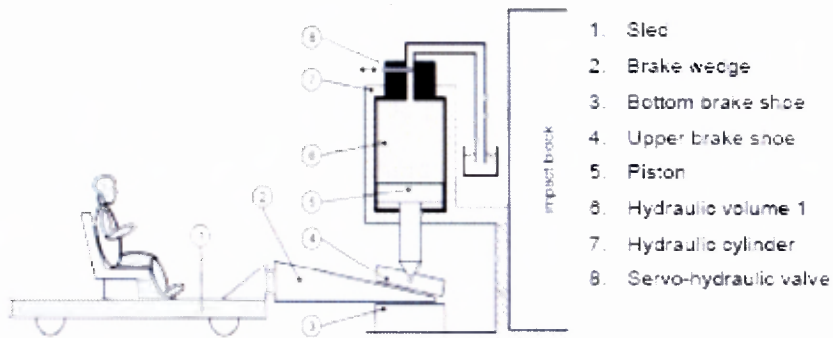


Figure 2-9: Schematic of MESSRING servo hydraulic crash testing system

As the sled approaches the deceleration end, the sled makes contact with the brake wedge which is located between a tapered brake shoe. The piston in the hydraulic cylinder will be retracted at a rate which is prescribed. The friction between the brake wedge and the brake shoe will slow the sled down by transferring the deceleration loads onto the sled system. The control system can vary the input pulse to the hydraulic cylinder to obtain the desired deceleration profiles. The braking distance is 1.8m and the maximum achievable deceleration is 70g [9].

2.5.1.1 Alternative MESSRING deceleration systems

MESSRING have other options available for the braking system in addition to the one discussed above. The first alternative option is a method which involves using polyurethane (PU) tubes. A number of PU tubes would be fixed to a robust steel frame or concrete block at the deceleration end. The brake mandrels or “olives” are connected to a steel plate that fits on the flange on the front end of the sled. When contact is made between the mandrels and the PU tubes, the friction generated slows the sled down. Each tube is capable of a 100kN braking effort [1]. A schematic of the braking system is shown in figure 2-10.

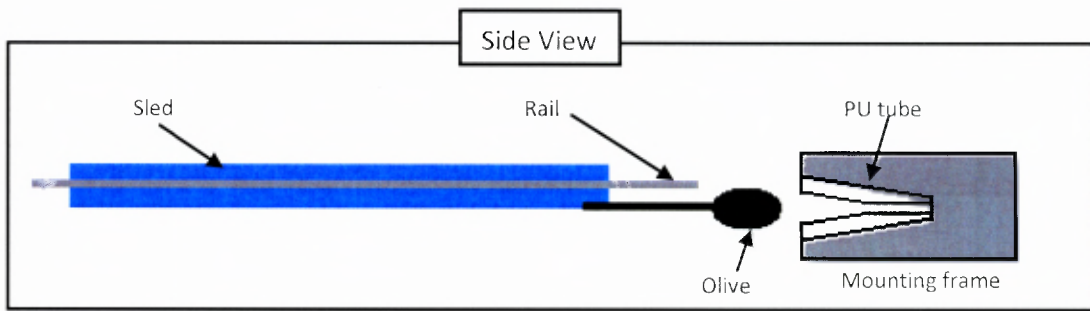


Figure 2-10: Polyurethane (PU) tube braking

The second alternative method of braking is one that utilises the bending of steel bars. It uses steel bars drawn through actuated rollers (see figure 2-11). This method can achieve a braking effort of up to 2MN over a distance of 1.5m [1].

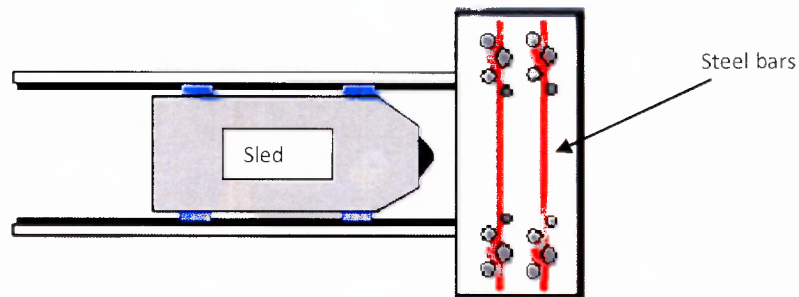


Figure 2-11: Schematic of steel bar braking

2.5.1.2 Deceleration considerations of BISRU

The PU tube and steel bar strain energy method were both considered for the braking system for the BISRU Sled Tester. The PU tube method was decided against, since the magnitudes of the deceleration forces are very dependent on the mechanical properties of the polyurethane, which fluctuate with respect to temperature [3]. The relative force magnitudes are also relatively high, making the deceleration resolution low [3]. These limitations put into question the control and repeatability of the tests that can be performed. The steel bar strain energy method was not used since this requires the destruction of steel tubes that will have to be replaced for each test. This requires an unacceptable amount of setup time between tests and moreover, it would be costly to keep replacing steel bars for each test. The clamping method was also an area of concern. A third method was also considered for the BISRU deceleration system and this entailed using magnetic eddy currents to slow the sled down. The concept involved an array of magnets